Autonomous Motion of Metallic Microrods Propelled by Ultrasound

Wei Wang,[†] Luz Angelica Castro,[‡] Mauricio Hoyos,[‡,*] and Thomas E. Mallouk[†,*]

[†]Department of Chemistry, The Pennsylvania State University, University Park, Pennsylvania 16802, United States and [‡]Laboratoire de Physique et Mécanique des Milieux Hétérogènes, UMR7636 CNRS, UMPC, ESPCI, 10 rue Vauquelin, 75005 Paris, France

ABSTRACT Autonomously moving micro-objects, or micromotors, have attracted the attention of the scientific community over the past decade, but the incompatibility of phoretic motors with solutions of high ionic strength and the use of toxic fuels have limited their applications in biologically relevant media. In this letter we demonstrate that ultrasonic standing waves in the MHz frequency range can levitate, propel, rotate, align, and assemble metallic microrods (2 μm long and 330 nm diameter) in water as well as in solutions of high ionic strength. Metallic rods levitated to the midpoint plane of a cylindrical cell when the ultrasonic frequency was tuned to create a vertical standing wave. Fast axial motion of metallic microrods at ~200 μm/s was observed at the resonant frequency using continuous or pulsed ultrasound. Segmented metal rods (AuRu or AuPt) were propelled unidirectionally with one end (Ru or Pt, respectively) consistently forward. A self-acoustophoresis mechanism based on the shape asymmetry of the metallic rods is proposed to explain this axial propulsion. Metallic rods also aligned and self-assembled into long spinning chains, which in the case of bimetallic rods had a head-to-tail alternating structure. These chains formed ring or streak patterns in the levitation plane. The diameter or distance between streaks was roughly half the wavelength of the ultrasonic excitation. The ultrasonically driven movement of metallic rods was insensitive to the addition of salt to the solution, opening the possibility of driving and controlling metallic micromotors in biologically relevant media using ultrasound.

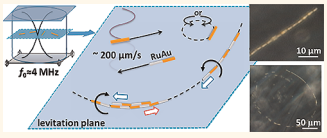

KEYWORDS: ultrasonic standing wave · metallic microrod · autonomous motors · self-assembly · self-acoustophoresis

Synthetic micromotors are an emerging class of micromachines.[1−3] The micromotors studied so far have been driven by a variety of mechanisms, including electrochemical decomposition of chemical fuels,[4−9] magnetic fields,[10−15] magnetic interactions between particles,[16] electric fields,[17,18] light,[19−22] bubble-driven propulsion,[23−26] polymerization,[27] and diffusiophoresis.[21,28,29] Micromotors fall into two classes: they can be propelled by external (*e.g.*, electric or magnetic) fields, and therefore move in concert with each other, or they can be propelled by local conversion of energy and move autonomously. Autonomous micromotors display fascinating biomimetic behavior that includes transport of cargo,[30−33] chemotaxis,[34] swarming, and predator−prey interactions,[21,35] and they have been studied for possible applications in bioanalytical sensing and microfluidics.[9,36−38] However, for motors that can move autonomously, there are issues that limit their practical utility in biological environments. Many catalytic micromotor systems rely on the use of toxic hydrogen peroxide (H_2O_2) or hydrazine derivatives as the fuel.[7−9,23−26,30−33] In addition, the high ionic strength of biological fluids is incompatible with propulsion mechanisms based on electrophoresis and diffusiophoresis.[5,8,10,11,17,24,26,29] While external electric and magnetic fields can be used to drive micro-objects in biological media, the resulting motion is not autonomous. Given the current strong interest in microrobotics for medical diagnostics, drug delivery, and minimally invasive surgeries, there continues to be a need for a biocompatible energy transduction mechanism that can power autonomous micromotors.[1,39,40]

Acoustic energy is an interesting candidate for driving micromotors in fluids, including biological media. Medical applications of sound waves at high frequency, such as ultrasonography, have been developed for decades and are widely used.[41] High frequency sound waves, in particular in the MHz regime, have minimal deleterious effects on biological systems.[42,43] Not only are sound waves in this frequency range safe, they are also a powerful tool for manipulating microparticles. Built upon the experimental discoveries of the acoustic collection of small suspended particles in the early 19th century by Kundt and Lehman,[44] and subsequent theoretical work,[45−47] the understanding of the ultrasonic standing wave and technological advancements in ultrasonic transducers have made more advanced manipulation of suspended microparticles possible.[48−56] For example, suspended microscale spherical particles can be aligned into 1-D lines,[49,50,55] 2-D arrays, and more complicated patterns.[48,52]

* Address correspondence to hoyos@pmmh.espci.fr, tem5@psu.edu.

Received for review March 24, 2012 and accepted May 25, 2012.

Published online May 25, 2012
10.1021/nn301312z

The 3-D manipulation of microparticles has also been achieved by using the appropriate experimental geometry.[56] This kind of positioning, regardless of its dimensionality (1-, 2-, or 3-D) or how the acoustic field is applied (surface acoustic wave or bulk acoustic wave), is usually considered to be the result of collecting microparticles at the nodes of ultrasonic standing waves, and the motion of the particles is driven by a pressure gradient. Acoustic levitation and streaming are also commonly observed during these experiments. They can be attributed to the primary acoustic radiation force and to steady-state fluid flow caused by the variation of the acoustic field, respectively.[53,57] Another interesting aspect of research in this field is the ability to align high aspect ratio particles, such as rods and tubes,[58−60] and to rotate particles by using acoustic fields.[61,62] However research in this area has so far been limited and autonomous microrod propulsion has not been reported.

Here we describe experiments in which ultrasonic acoustic waves can propel metallic rods in fast (~200 μm/s) axial directional motion as well as in fast in-plane rotation. Additionally, we have observed the formation of ring and streak patterns by metal rods and the assembly of metallic rods and spheres into well-aligned chains, as well as their rotation. The key findings of these experiments are as follows: (1) metallic rods, particularly polar metallic rods, behave differently in acoustic fields than polymer spheres or rods; (2) shape asymmetry drives motion along the axis of the metallic rod, a mechanism we tentatively call self-acoustophoresis; and (3) the presence of metallic rods at the edge of a ring or streak pattern in the nodal plane induces strong vortices in the fluid, which causes the rods to spin and results in their self-assembly into chains.

RESULTS AND DISCUSSION

Experiments were conducted using a homemade cylindrical cell, as illustrated in Figure 1, and videos were taken with an optical microscope (see Supporting Information). Particle motion in the cell was typically observed in dark field.

The conditions for forming a standing wave in this cell are described by eq 1,

$$h = \frac{1}{2}n\lambda = \frac{1}{2}n\frac{c}{f}, \quad n = 1, 2, 3... \qquad (1)$$

where h is the cell height (acoustic path length) and c is the speed of sound in the medium (deionized water, c = 1492 m/s). The cell was designed to have a height of 180 μm. For the simplest case where n = 1, the resonance frequency is calculated from (1) to be 4.1 MHz, and at that frequency a nodal plane forms at the center of the cell where the acoustic pressure is at its minimum (Figure 1, inset). Preliminary experiments indicated a resonant frequency of about 3.7 MHz.

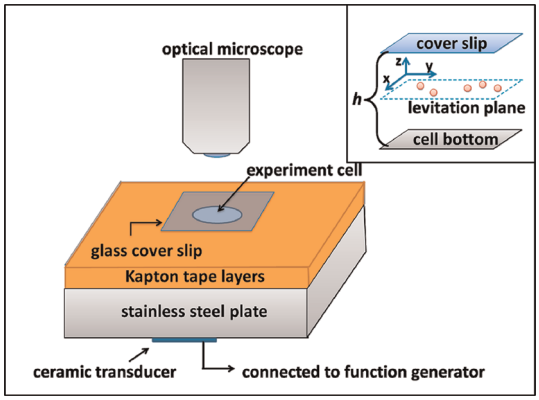

Figure 1. Cylindrical ultrasonic cell. The transducer was mounted on a steel plate at the bottom of the cell. Inset: Illustration of the cell cross-section when the acoustic field is applied. The particles are shown in the levitation plane. The cell height, *h*, is defined as the distance between the top coverslip and the bottom wall of the cell.

Therefore sine waves with a frequency of 3.7 MHz and output amplitude of 10 $V_{p\text{-}p}$ (a output power of 23.97 dBm, or 249.5 mW) were typically used as the starting point for experiments, and both parameters were varied continuously. Experiments were also done in pulse mode, where the acoustic power was delivered at the same instantaneous power and frequency, but in trains of pulses. A number of pulses N was delivered over a period of time T_p, where $T_p = N/f$ and f is the frequency. These pulse trains were separated by a repetition time T_r. The *duty cycle D* is defined by $D = T_p/(T_p + T_r)$.[63] The number of pulses N was varied between 150 and 800, and the pulse repetition rate ($1/(T_p + T_r)$) was varied from 1 to 4 kHz. This is illustrated in Figure S12 (see Supporting Information).

Spherical Polystyrene Particles. Experiments were first conducted with polystyrene microspheres (470 nm and 2 μm diameter) to gain an understanding of the motion of spherical particles in the cylindrical acoustic cell. FESEM images of the polystyrene particles are shown in the Supporting Information (Figure S1 and S2). In the absence of ultrasound, colloidal particles suspended in the cell showed ordinary Brownian motion (Supporting Information video S1, part 1), and there was little evidence of interparticle or particle−substrate (steel plate) interactions at the particle densities used. Upon application of bulk acoustic waves at 3.7 MHz, the polystyrene particles levitated into the nodal plane (also called the levitation plane), as evidenced by the fast upward motion of all the particles from the bottom of the cell. The origin of the levitation force is well-known in the acoustics literature, and is generally attributed to the primary acoustic radiation force exerted on particles by sound propagation perpendicular to the substrate.[64] Since the acoustic pressure is at its minimum in the nodal plane, particles are trapped in that plane. The frequency range for levitating particles was between 3.5 and

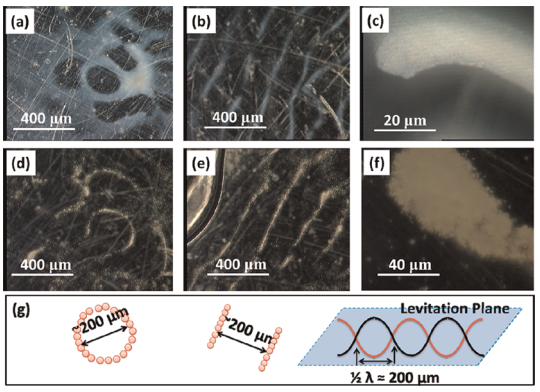

Figure 2. Typical patterns formed by polystyrene (PS) tracer particles in the nodal plane in a 3.7 MHz acoustic field. (a−c) ring patterns, streak patterns, and a dense aggregate formed by 470 nm diameter PS particles, respectively. (d−f) the same types of patterns formed by 2 μm diameter PS particles. In these dark field images, the particles appear bright and the background is dark. (g) Cartoons showing the dimensions of the formed patterns as well as the nodes.

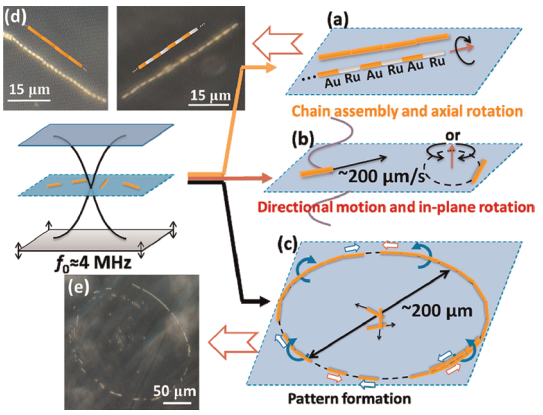

Figure 3. (a)-(c): Illustration of the kinds of motion (axial directional motion, in-plane rotation, chain assembly and axial spinning and pattern formation, especially ring patterns) of metal microrods in a 3.7 MHz acoustic field. AuRu rods (gold−silvery color in dark field) showed similar behavior to the Au rods, except that they moved with their Ru ends (the silvery end in the image) forward and aligned head-to-tail into chains. (d) and (e): Dark field images of typical chain structures and ring patterns formed by Au and AuRu rods. Note that the cartoons superimposed on (d) are intended to show the alignment of the rods and are not to scale or in proportion to the aspect ratio of the Au or AuRu rods.

4 MHz, which was close to the calculated $n = 1$ resonant frequency of the cell. When frequencies below or beyond that range were used, the particles remained at the bottom of the cell. Turning off the acoustic excitation resulted in sinking of the levitated particles.

Once in the nodal plane, both small (470 nm) and large (2 μm) spherical polystyrene particles showed acoustic streaming. At certain frequencies, within seconds to minutes, the particles formed circular or linear aggregates (termed ring and streak patterns, respectively, in the discussion below), as shown in Supporting Information video S2 and Figure 2. It was hard to predict or control the shapes of these aggregates, although varying the frequency could lead to the transformation from streak patterns to ring patterns, or *vice versa*. The collection of particles in patterns in the nodal plane of a bulk acoustic field has been reported before and is generally considered to be due to the variation of the acoustic field in the lateral directions.[57,65] Such variations can arise from near field effects or from higher dimensional acoustic modes.[66,67] Although the origin of these variations is not known in the present case, it appears that the particles follow the acoustic energy distribution in the nodal plane.

The ring diameters and distances between streaks were typically in the range of 200 μm, which corresponds to half the wavelength of the sound wave at the driving frequency. This indicates a correlation between the patterns and the acoustic nodal structures in the plane (Figure 2g). Although sharp resonance patterns are difficult to obtain in the nodal plane because of scattering and reflection of acoustic waves, under certain conditions localized nodal patterns can be formed, and that explains the ring and streak patterns that formed at certain frequencies. One can draw a comparison between the patterns seen in Figure 2 to nodal patterns formed by sand on a Chladni plate, which collects mobile particles at the acoustic nodes.[68] Similarly, 2-D alignment of particles into rings and other more complicated structures has been experimentally demonstrated and theoretically modeled.[52] It is worth noting that once the polymer microparticles were collected and aligned into rings or streaks, they showed only acoustic streaming with no evidence of powered rotation or directional motion in either the levitation plane or the vertical direction.

Metallic Microrods. Suspensions of metallic microrods showed interesting differences from polymer spheres under the same conditions. In these experiments, the rods were typically 1−3 μm long and 300 nm in diameter. FESEM images of the metal rods are included in the Supporting Information. The rods were made of a single metal component (Au, Ru, or Pt) or were axially segmented (AuRu or AuPt, with the two ends being different metals). Au, Ru, and Pt rods behaved almost identically to each other, and this was also true for AuRu and AuPt bimetallic rods. Therefore for the convenience of the discussion, we focus on pure Au and axially segmented AuRu rods. When the acoustic field was turned on, the rods levitated (Supporting Information Video S2, part 1) and ring and/or streak patterns were formed (Supporting Information Video S2, part 5−7), similar to those of polymer tracer particles. However a number of new behaviors (illustrated and summarized in Figure 3), including powered autonomous motion, were also observed.

Once in the levitation plane the metallic rods showed axial directional motion (Figure 3b) at speeds as high as ~200 μm/s, as can be seen in Supporting

Information Video S2, part 2. The directional motion of a few AuRu rods at the resonant frequency was tracked, and the trajectory is plotted in Supporting Information Figure S10. It is important to note that this motion was not driven simply by fluid convection, as rods that were near each other in the fluid moved autonomously in different directions. Varying the amplitude of the acoustic wave can lead to faster or slower rod speed. The speed was a function of both the location of the rods in the levitation plane and the frequency of the acoustic wave. For example, at a driving frequency of 3.776 MHz, the rods near the cell center showed very fast axial motion as well as in plane rotation (Supporting Information Video S2, part 3), while rods near the edge of the cell showed much slower motion. Therefore we identify 3.776 MHz as the resonance frequency for the cell center. It is important to note that even a slight deviation (a few kHz, about 1% of the frequency) away from the resonant frequency dramatically decreased the intensity of the rod motion. However tuning the frequency away from resonance for the cell center brought other parts in the cell into resonance and induced rapid movement of metal rods in those locations. Representative observations of this motion are shown in Supporting Information Video S2, part 2. Although we could not distinguish in the optical microscope which end was moving forward for single component metal rods, the two ends of the bimetallic rods had clear optical contrast in dark field, from which we could infer that they were propelled with one end consistently forward. For example, in the case of AuRu rods, the directional motion was always with the Ru end (which appears silvery in the dark field) leading. This suggests that the asymmetry of composition or shape of the metal rods can lead to directional motion.

Directional motion of metal rods occurred everywhere in the levitation plane, even where rods were aggregated into ring or streak patterns (Figure 3c). As noted above, the metallic rods when levitated into the nodal plane also formed ring and streak patterns. However unlike the polymer spheres, which showed only acoustic streaming within these patterns, metallic rods moved along the edges of these patterns and particularly for the ring patterns orbited the center of the ring, with different rods orbiting clockwise and counter-clockwise. This indicates that the propulsion of the metallic rods in the acoustic field is independent of their aggregation into rings or streaks; that is, the aggregation of the rods into patterns did not stop their directional motion or change their direction. Additionally, the metallic rods not only formed a dense ring pattern, as polystyrene particles did, but also populated the inside of the ring, forming many concentric and less dense rings in which chains of rods orbited the center (see Figure 3e and Supporting Information Video S2, part 5). At the centers of these rings, there was a smaller number of metal rods showing limited directional motion. As noted above for the case of polystyrene particles, the aggregation of metal rods into defined structures in the levitation plane can be attributed to the distribution of the acoustic energy in that plane.

Within the rings or streaks formed by metallic rods we observed another unique behavior that was not seen with spherical polymer particles. The metal rods and their aggregates rotated rapidly about the axis of the rods and the spindle axis of the rod-shaped aggregates, respectively, as is illustrated in Figure 3a. In contrast, for 470 nm and 2 μm diameter polymer spheres, we observed the aggregation of particles into patterns, but no axial rotation. Owing to the instrumental limitation of the camera used to record the videos (30 frames per second), the rotation speed of the metal rods or aggregates could not be accurately measured. At present, this motion is not completely understood, but it has been reported that ultrasound irradiating metal particles and cylinders in suspension can excite elastic surface waves, or Rayleigh waves, at frequencies spanning from kilohertz to megahertz depending on the nature of the metal.[69] Depending on the angle of the incident wave, in this case the standing wave in the levitation plane, the surface waves can have a helical shape with respect to the rod axis.[70] We hypothesize that the helical surface waves can drive the rotation of the metal rods, which in turn creates a vortex through hydrodynamic drag. It may also cause the in-plane rotation of metallic rods noted above (Figure 3b and Supporting Information Video S2, part 3), since in that case the incident wave is in the vertical direction, not in the levitation plane as it is for rods rotating axially. It is important to note that Rayleigh waves are also present in the case of spheres, generating rotation by interaction with incident standing waves. This will help explain the chaining and rotation of gold microspheres, which will be discussed below. This effect was seen only for metallic particles and not for polymer particles, presumably because the elastic waves in polymers are dampened much more effectively because of the higher compressibility of polymers.

For ring patterns, the vortices always pointed to the inside of the ring in the sense that fluid was driven into the ring from above and out from below, regardless of which direction the rods were moving or where they were observed on the ring. This toroidal motion can be seen in Supporting Information Video S2, part 6. This uniform flow pattern around the ring, concurrent with the axial movement of rods around the ring, indicates that the generation of vortices and the axial propulsion of the metal rods have two distinct mechanisms and can be decoupled.

To examine more closely the fluid flow induced by the spinning metal rods as well as to study the interaction between the metal rods and passive tracer

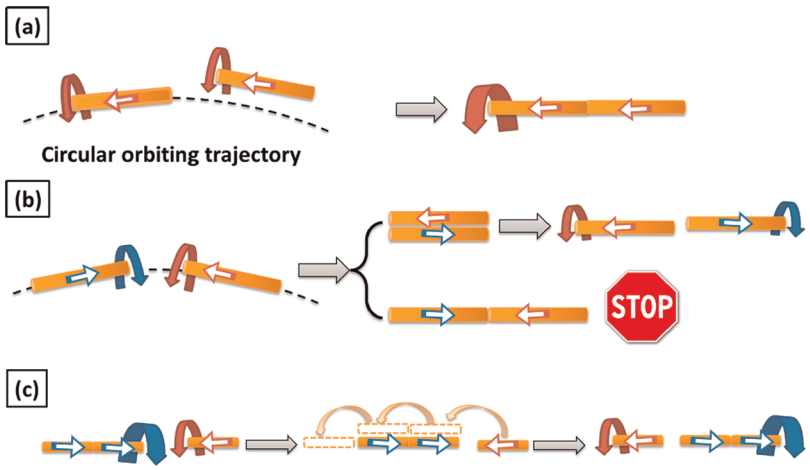

Figure 4. Illustration of chain assembly and directional motion of metal rods along the chains: (a) two metal rods moving in the same direction along the ring interacts and form a spinning doublet. (b) two metal rods moving in opposite directions either brush against each other or meet each other head-to-head (much less likely to occur); (c) when a metal microrod meets a chain moving in the opposite direction, the rod brushes against the chain and the two parties continue separately.

particles, we mixed metal rods with 470 nm polystyrene particles (see Supporting Information Video S3). The tracer particles were readily trapped by the vortex formed around the metal rods once the ring or streak patterns were established, and they were observed to orbit around the rod spindle axis. The hydrodynamic drag of the vortex extended many rod diameters into the fluid, and the vortex tended to become stronger as the spinning bundle increased in length and diameter. The motion of tracer particles in this experiment also confirmed the toroidal fluid pumping into and out of the ring.

The vortices generated by the metal rods lead to the self-assembly of the rods into chains, as illustrated in Figure 3(a) and (d), and in Video S2, part 4 as well as Video S4, part 5. The chaining occurred exclusively in the ring and streak patterns, and is believed to result (as described below) from a combination of several attractive and repulsive forces. Once two metal rods align, they continue to assemble with other rods, individual or chains, and form long chains. Interestingly, when two chains (or rods) traveling in opposite directions meet each other, they do not interfere with each other's motion or assemble into growing chains. Instead they spiral around each other and continue in their original direction of motion; these directions are opposite along the chain axis, because all the rods are confined by the vortex drag force. This illustrates the strong integrity of the self-assembled chain structures. Figure 4 schematically illustrates the self-assembly and interactions of chains formed by metal rods.

We also observed polar chains formed by AuRu bimetallic rods (Figure 3a,d). Each polar rod in these chains points in the same direction so that the chain has an AuRu|AuRu|AuRu|... structure. This head-to-tail assembly is not particularly surprising considering that the bimetallic rods always move with the same end forward (*e.g.*, the Ru end for AuRu rods), and only rods moving in the same direction can align into chains. As noted above, chains moving in opposite directions eventually pass each other without coalescing into a single chain.

Metallic Spheres and Polymeric Rods. To better understand the effects of different materials and shapes in the ultrasonic field, we conducted control experiments with polymer (polypyrrole) rods and gold microspheres. The behavior of these particles is summarized briefly in Table 1.

To summarize the results collected in the table, metal rods induced strong vortices when aligned and also showed strong axial directional motion, whereas spherical metal particles induced vortices but only rarely showed directional motion, which was possibly a consequence of some small shape asymmetry. Polymer particles, regardless of their shape, did not show directional motion or induce strong vortices. This supports the hypothesis that material and shape are important in inducing strong vortices and directional motion. In addition, the fact that polymer rods showed no directional motion but weak axial rotation when aligned supports the hypothesis that axial rotation and directional motion are distinct behaviors that arise from different effects in the acoustic field.

Among the kinds of motion described above, axial propulsion is particularly interesting because it opens up the possibility of powering autonomous movement in a variety of media that are compatible with ultrasound. The speed of axial propulsion can be altered by changing the amplitude and the frequency of continuously applied acoustic energy. Another way to change the activity of the acoustic motors, and to estimate the magnitude of forces that cause levitation, chain formation, and axial motion, is by using pulsed ultrasound. Pulsed-mode experiments were carried

TABLE 1. Summary of Behaviors of Different Samples in an Acoustic Field

sample	pattern formation[a]	directional motion	particle alignment into chains[c]	aggregate spinning
polymer spheres	yes	no	no, particles were loosely aligned into narrow aggregates	no
polymer rods	yes	no	no, particles were loosely aligned into narrow bands	yes, but weak
metallic spheres	yes	some did[b]	yes, with clear attraction between particles	yes, fast
metallic rods	yes	yes	yes, very regular chains were formed, clear attraction between particles observed	yes, fast

[a] Patterns formed by either polymer or metallic microparticles in an acoustic field are generally rings, streaks, or dense aggregates. [b] A small percentage of gold microspheres showed fast directional motion in an acoustic field. It is likely that these gold particles were not perfectly spherical (as can be seen in Supporting Information, Figure S3), and that their asymmetric shapes induced directional motion as in the case of gold rods. [c] See Supporting Information, Figure S11.

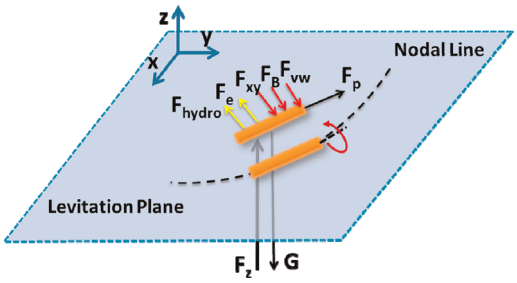

Figure 5. Illustration of the forces experienced by a metal rod in an acoustic field during self-assembly into chains. Red and yellow colors denote forces that bring the rods closer and push them apart, respectively. F_z, the primary radiation force in the z direction; G, the gravitational force; F_p, the propulsion force; F_{hydro}, the hydrodynamic force from the vortex; F_e, the electrostatic force; F_{xy}, the transverse component of the primary radiation force in the levitation plane; F_B, the Bjerknes force; F_{VW}, the van der Waals force.

out at the same frequency and amplitude as in the continuous experiments. The threshold for levitating rods at the onset of rotating motion was at a duty cycle of $D_0 = 0.04$, which translates to a 1 kHz pulse repetition rate and $N = 150$. By choosing different combinations of T_r and T_p, and therefore different D, it was possible to observe the onset of different kinds of movement. For example at a high D, which means a larger T_p and smaller T_r, metal rods levitate and show strong rotation. However when D is lowered, the activity of the rods decreased until at the threshold D_0 the rods maintained levitation but showed little rotation. A duty cycle below the threshold D_0 results in destabilization and sinking of the rods back to the bottom of the cell. Supporting Information, video S5 demonstrates a pulse mode experiment with metal rods at a small pulse repetition rate.

Discussion of Forces at Work. The results from the pulsed-mode experiments help to quantify the forces at work in the different motions of the metal rods, especially the self-assembly into spinning chains (Figure 5). First, there is a primary radiation force (PRF) in the z direction (F_z) that levitates the rods and pushes them into the nodal plane at the center of the cell. Below the threshold duty cycle of $D_0 = 0.04$, metal rods were no longer levitated and began to sink. At this power, the levitation force balances the gravitational force (G), which is approximately 0.027 pN for 2 μm $\times$ 300 nm gold rods. Therefore, for experiments carried out with continuous ultrasound at the same instantaneous power, the levitation force in the z direction can be estimated to be $1/D_0 \times 0.027$ pN = 0.75 pN.

There is also a transverse component of that primary radiation force acting on the rods in the xy levitation plane (F_{xy}), which pushes them into nodal lines and forms the streak and ring patterns in the levitation/nodal plane. At low Reynolds numbers ($\sim 10^{-4} - 10^{-5}$ for microrods moving at a few μm/s), this force is equal to the hydrodynamic drag force, which can be estimated from eq 2.

$$F_{drag} = \frac{2\pi\mu L}{\ln\left(\frac{2L}{R}\right) - 0.72} v \qquad (2)$$

where μ is the dynamic viscosity of water, L is the length of the rods (2 μm), R is the radius (150 nm), and v is the velocity of the rods that are being pushed to the nodal lines, which is as $\sim$5 μm/s as seen in the video clips. From eq 2, the drag force calculated to be $\sim$0.025 pN, which equals to the transverse primary radiation force F_{xy}. The 1−2 orders of magnitude difference between the primary radiation force in the z direction (0.75 pN) and the xy direction (0.025 pN) is consistent with previous experiments in similar geometries.[71]

The force that propels the metal rods along their axis (F_p) can also be estimated from eq 2, only in this case the velocity v can be as high as 200 μm/s, which corresponds to a force of 0.98 pN. This force is about 2 orders of magnitude stronger than F_{xy} and is comparable to the primary radiation force in the z direction F_z. This suggests the axial propulsion of the metal microrods arises primarily from scattering of acoustic waves traveling in the z-direction. A more detailed discussion on the axial propulsion will be provided in the following section.

It is well-known that for two particles in the same nodal plane there exists an attractive force between the particles that arises from the reflected wave from one particle acting on the other. This is known as the secondary radiation force, also called the Bjerknes force (F_B). Woodside *et al.* measured the Bjerknes force relative to the primary radiation force in the z direction for two 5.1 μm radius polystyrene particles and found that the maximum F_B is approximately 2 orders of magnitude weaker than the maximum F_z.[65] Using their

experiment as a guideline we estimate the average Bjerknes force between two metal rods to be the order of 10^{-2} pN, which is similar to the transverse component of the primary radiation force F_{xy}. We note that F_B scales as $1/D^2$, where D is the distance between the particles. Therefore as the rods get closer to each other they experience a stronger F_B.

Another attractive force is the van der Waals force (F_{VW}), which is significant only at short-range. By approximating the particles as 1 μm diameter gold spheres, we estimate F_{VW} on the order of 10^{-2} pN at $D = 1$ μm from

$$F_{VW} = \frac{AR}{12D^2} \quad (3)$$

Here A is the Hamaker constant for gold (3.0×10^{-19} J), R is the radius of the particle (500 nm), and D is the distance between the particles. Since F_{VW} is on the same order of F_B, they play similar roles in bringing two rods together when they are relatively close.

For metal rods that have a negative zeta potential in water, there is additionally a longer-range electrostatic repulsive force (F_e). As detailed below, we compared the behavior of the metal rods in pure water and in solutions of high ionic strength in which the electrostatic attraction should be screened at distances greater than tens of nanometers. Because the behavior was similar in the two media, it appears that the effect of electrostatic repulsion in the chain assembly process is negligible.

Considering the magnitude and direction of these forces, we present the following scenario for the self-assembly of metal rods: two rods moving near the nodal line are pushed by the transverse primary radiation force (F_{xy}) so that they align on the nodal line, preferentially into one line so each rod is at the pressure minimum. When rods align within a distance of a few micrometers, the attractive Bjerknes (F_B) and van der Waals (F_{VW}) forces cause them to accelerate toward each other and form a chain. The spiral trajectory of the rods moving together and eventually connecting to form a spinning chain on the nodal line, as shown in Supporting Information, Video S2 part 4, is a combination of the axially forward motion of the incoming rod and its circular revolution around the chain.

Mechanism of Axial Rod Propulsion. At present, the axial motion of the metallic rods is not understood quantitatively, but some mechanisms can be eliminated based on control experiments. One of these is self-electrophoresis, which is one of the most important mechanisms for catalytic microparticle propulsion in the presence of chemical fuels such as H_2O_2.[72,73] Because the generation of H_2O_2 in water by ultrasound has been reported,[74] it is conceivable that H_2O_2 generated at the rod surface could contribute to axial motion. However three experimental observations argue compellingly against this mechanism in the present case. The first one is that single-component rods, such as Au and Ru, showed comparable directional motion to bimetallic AuRu rods; the former do not show fast chemically powered movement in H_2O_2 solutions, whereas the latter do. The second observation is that AuRu moved with the Ru end forward when powered by ultrasound and in the opposite direction when powered by H_2O_2.[72] We observed that these rods reversed their direction when an acoustic field was applied to a rod suspension in 5% H_2O_2 solution, indicating different mechanisms with and without the acoustic field. It is also well-known that even low concentrations of salts inhibit the self-electrophoretic movement of catalytic micromotors in H_2O_2.[8] However, we observed identical behavior when the acoustic experiments were conducted in 1, 10, or 100 μM $NaNO_3$ solutions, while the catalytic motors showed significantly decreased activity in 100 μM $NaNO_3$. We also found that the activity of levitated metal rods in ultrasound was not significantly affected in a phosphate buffer saline (PBS) solution diluted 1:1 with water. The latter experiment illustrates the promise of using ultrasonic propulsion of metal rods in a biological environment.

A more plausible mechanism for the directional motion of metal rods in an acoustic field is based on the shape asymmetry of the rods. Nanorods prepared

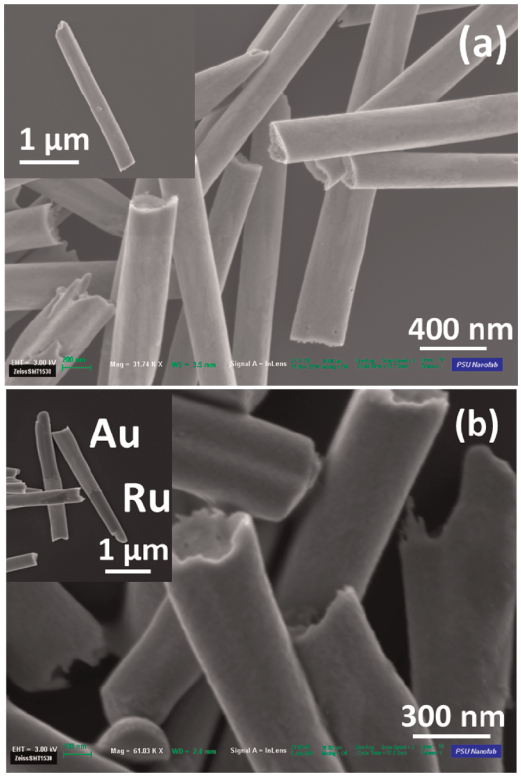

Figure 6. Electron micrographs of Au (a) and AuRu (b) rods used in the ultrasonic propulsion experiments. For AuRu rods, the Au end is clearly concave and there is also some incidence of rod branching at the Au end. The Ru end is usually pointed or flat. Au rods typically have one concave end and one pointed or flat end.

by template electrodeposition typically have a concave or convex end instead of perfectly flat end. The pores in which the nanorods are grown are small enough that the rod−wall interaction can lead to preferential growth along the wall. The unevenness of the surface on the rod end is made more complex by the kinetics of the metal deposition, since fast growth (high current density) produces rougher deposits while slower deposition tends to produce a smoother end surface.[75,76] Field emission SEM images of the metal rods that were used in the acoustic experiments (Figure 6 and FESEM images in the Supporting Information) showed that regardless of the metals used, one end of the rod was always markedly concave while the other end was slightly convex to flat (Ru), fairly flat (Pt) or quite rugged (Au). The end where it was always concave was identified as the end grown immediately after deposition of the sacrificial silver layer, which is typically the first step in electrodepositing nanowires in AAO membranes.

The asymmetric shape of the metal rods can lead to an asymmetric distribution of the acoustic pressure from the scattering of the incident acoustic waves at the metal surface. The scattering of acoustic waves from concave shapes concentrates energy near the curvature, whereas convex shapes scatter radially and weaken the energy density near the curvature. Therefore asymmetric shapes result in an uneven distribution of acoustic pressures in the fluid that is stronger at the concave end (Au end in AuRu rods), propelling the rods with the other end (Ru) consistently forward. It is important to note that many studies have been made about scattering of acoustic waves by cylinders at $ka > 1$ (where k is the wavenumber and a is the cylinder diameter),[70,77] and only a few of them focus on cases where $ka \ll 1$,[78,79] which is the case in the present experiments.

The locally induced pressure gradient propels the metal rods in a similar way as the acoustic pressure gradient moves particles, a phenomenon sometimes called acoustophoresis.[48,80] Since the pressure gradient is generated locally and affects only the individual rods, we use the term self-acoustophoresis to describe this mechanism. We also examined AuPt bimetallic rods and the same mechanism could be applied to explain their direction of motion. Although we cannot identify which end leads the directional motion of single-component metal rods, the same concave features were found on those rods, and therefore their motion can be explained by the same mechanism.

To further investigate this mechanism, we fabricated PtAu wires by electrodepositing Pt before Au segment. Rods made this way had a concave end at the Pt end, as shown in Supporting Information, Figure S4b. In this case, some of the PtAu rods moved with the Pt end forward while others moved with the Au end forward. The reversal of direction of some of the rods supports the hypothesis that the concave feature at the end of the rods is responsible for axial propulsion.

Finally, for ultrasonically propelled micromotors to be useful in biological environments, it is important to evaluate whether the power level is harmful to tissues or cells. The output power from the function generator in a typical experiment is 250 mW. A fraction of this power is transmitted to the sample cell (0.2 cm^2), and the rest is dissipated by the much larger steel plate (20 cm^2) that is coupled to the transducer. While we have not quantified the power density inside the fluid cell, the upper limit is 250 mW/0.2 cm^2 = 1.25 W/cm^2. That power level is intermediate between that of therapeutic ultrasound (several W/cm^2 or higher) and diagnostic ultrasound (740 mW/cm^2, the maximum ultrasonic power level allowed by FDA for diagnostic purposes).[81,82] Because the configuration of our transducer and cell are not yet optimized, it seems reasonable to conclude that fast propulsion of metallic micromotors will be possible within the power limits of diagnostic ultrasound.

CONCLUSIONS

We have demonstrated that MHz frequency acoustic waves can propel, align, rotate, and assemble metallic microrods in water. Control experiments with polymer particles and metal spheres lend support to the hypothesis that shape and material play a critical role in the directional motion and the generation of strong vortices along the axis of aligned metal rods. The fact that axial movement and chain assembly/spinning were observed independently of each other in experiments with metal and polymer rods indicates that the two kinds of movement are caused by distinct effects. On the basis of observations with template-grown homogeneous and bimetallic nanorods, it is likely that shape asymmetry, specifically the curvature at the ends of the microrods, leads to the directional motion by a self-acoustophoresis mechanism. The significance of this finding lies in the possibility of driving and controlling micromachines in biologically relevant environments using ultrasound.

MATERIALS AND METHODS

Sample Preparation. Polystyrene microspheres of 470 nm were purchased from Polybead (cat. no. 07763, amino-functionalized). Polystyrene microspheres of 2 μm were purchased from Polysciences (cat. no. 18327, carboxylate-functionalized). Gold microparticles (AuMP, 0.8−1.5 μm, 99.96+ %) were purchased from Alfa Aesar. The synthetic procedure for growing microrods was adapted from previous reports.[72,83−85] Anodic alumina membranes (AAO, purchased from Whatman Inc., 200 nm pore size) were used as the template for the electrodeposition of

metals. The metal plating solutions were purchased from Technic Inc. and were used as received. A 5 nm length of Cr and 350 nm of Ag were evaporated by using a Kurt Lesker Lab-18 electron beam evaporator on the back side of the AAO membrane (branched side) to serve as the working electrode. A Pt coil was used as the counter electrode. For the deposition of Ag, Au, or Pt, a two-electrode system was generally used with the Pt coil serving as the pseudoreference electrode. In this case, current was controlled to be constant. For the deposition of Ru and polypyrrole, a three electrode system with Ag/AgCl in 3 M NaCl as the reference electrode was used, and rods were grown at constant potential. In a typical deposition procedure, a $\sim$10 μm silver segment was first deposited into the AAO membrane as the sacrificial layer. Then segments of metals (or polymers) of interest were grown. The lengths of the segments were controlled by monitoring the charge passed. The plating conditions for Ag, Au, and Pt were -1.77, -1.24, and -1.77 mA/cm^2, respectively. Ru and polypyrrole were deposited at a constant potential of -0.65 V and $+0.7$ V *vs* Ag/AgCl, respectively. Note that at the potential to deposit polypyrrole, silver is oxidized and dissolved, and therefore in this case a short gold plug was plated in the membrane instead of silver sacrificial layer. Multisegment nanowires were made by replacing the plating solution without disassembling the plating cell, with a rinsing step in between. After the electrodeposition step the membrane was thoroughly rinsed with DI water and dried, and usually one-half of the membrane was soaked sequentially in 1:1 v/v HNO_3 and 0.5 M NaOH to dissolve the silver and the alumina membrane, respectively. After that the wires were sonicated and washed in DI water several times until the pH was neutral. The nanowire suspension obtained from this procedure had a number density of around 1×10^9/mL.

A PBS buffer solution was made by dissolving 1 bag of commercially available BupH phosphate buffered saline pack (Thermo Scientific, no. 1890535) in 500 mL of DI water. The resulting solution contains 0.1 M phosphate and 0.15 M NaCl, and has a pH value of 7.2.

Acoustic Experiments. The acoustic experiment was conducted using a homemade cylindrical cell. The cell was made by applying three layers of polyimide Kapton tape (50 μm thickness per layer), with a circular hole of 5 mm diameter cut in the center, on a piece of stainless steel plate (45 mm $\times$ 45 mm $\times$ 1 mm). A ceramic transducer PZ26 (Ferroperm, Kvistgard, Denmark) was attached by conductive epoxy glue (Chemtronics ITW, Kennesaw GA, USA) to the back of the metal plate to generate acoustic waves in the thickness mode. The transducer was connected to a function generator that outputted sine waves (5062 Tabor Electronics, Israel), and the signal was amplified if necessary by a dual differential wide band 100 MHz amplifier (9250 Tabor Electronics, Israel). The signal was visualized with a digital storage oscilloscope (IDS 8064 60 MHz ISOTECH, Hanan, Israel). In a typical experiment, 30 μL of colloidal particle suspension was added to the cell, which was then covered by a square glass coverslip which served as the sound reflector. In the case of metal rods, the suspension normally had a number density of approximately 1×10^8 mL^{-1}. Video recording was started at the same time the function generator signal output was turned on. An Olympus BX60 M optical microscope and a commercial video capturing bundle (Dazzle Video Creator Plus) were used for observing the particles and recording videos.

Tracking of Particles in an Acoustic Field. The method of tracking the motors was based on our previous work on catalytic nanomotors.[72] Videos of the metal rods were captured at 30 frames per second. The video was then loaded with PhysMo 2, an open source tracking software (PhysMo—Video Motion Analysis Package, http://physmo.sf.net), and the coordinates of the metal rods as a function of time were recorded. Further data analysis was done in Microsoft Excel 2010. Rod speed was calculated by dividing the displacement of the rod center between two frames by the time interval (0.033 s), then taking the average of the speed over the selected tracking period. The tracking was repeated with multiple wires to ensure statistically robust results. An example of the tracking results and trajectories of six AuRu rods at the resonance frequency (3.700 MHz) are shown in Supporting Information, Figure S10.

Conflict of Interest: The authors declare no competing financial interest.

Acknowledgment. We thank Profs. Jay Maynard, Vincent Crespi, and Tony Jun Huang for helpful discussions. Work at Penn State was supported by the National Science Foundation under MRSEC Grant DMR-0802404. M.H. and A.C. acknowledge the financial support BDI from CNES-CNRS and Aide à la Recherche Grant CNES-France. Analytical instrumentation used in this work was supported by the Pennsylvania State University Materials Research Institute Nanofabrication Laboratory under National Science Foundation Cooperative Agreement No. ECS-0335765.

Supporting Information Available: FESEM images of microparticles, representative tracking results of AuRu microrods in an acoustic field, optical images of chains formed in four different experiments, and videos of particle movement in acoustic fields. This material is available free of charge *via* the Internet at http://pubs.acs.org.

REFERENCES AND NOTES

1. Mirkovic, T.; Zacharia, N. S.; Scholes, G. D.; Ozin, G. A. Fuel for Thought: Chemically Powered Nanomotors Out-Swim Nature's Flagellated Bacteria. *ACS Nano* **2010**, *4*, 1782–1789.
2. Wang, J.; Manesh, K. M. Motion Control at the Nanoscale. *Small* **2010**, *6*, 338–345.
3. Mallouk, T. E.; Sen, A. Powering Nanorobots. *Sci. Am.* **2009**, 72–77.
4. Liu, R.; Sen, A. Autonomous Nanomotor Based on Copper−Platinum Segmented Nanobattery. *J. Am. Chem. Soc.* **2011**, *133*, 20064–20067.
5. Pantarotto, D.; Browne, W. R.; Feringa, B. L. Autonomous Propulsion of Carbon Nanotubes Powered by a Multienzyme Ensemble. *Chem. Commun. (Cambridge)* **2008**, 1533–5.
6. Mano, N.; Heller, A. Bioelectrochemical Propulsion. *J. Am. Chem. Soc.* **2005**, *127*, 11574–11575.
7. Kline, T. R.; Paxton, W. F.; Mallouk, T. E.; Sen, A. Catalytic Nanomotors: Remote-Controlled Autonomous Movement of Striped Metallic Nanorods. *Angew. Chem.* **2005**, *117*, 754–756.
8. Paxton, W. F.; Baker, P. T.; Kline, T. R.; Wang, Y.; Mallouk, T. E.; Sen, A. Catalytically Induced Electrokinetics for Motors and Micropumps. *J. Am. Chem. Soc.* **2006**, *128*, 14881–14888.
9. Wu, J.; Balasubramanian, S.; Kagan, D.; Manesh, K. M.; Campuzano, S.; Wang, J. Motion-Based DNA Detection Using Catalytic Nanomotors. *Nat. Commun.* **2010**, *1*, 36.
10. Zhang, L.; Abbott, J. J.; Dong, L.; Peyer, K. E.; Kratochvil, B. E.; Zhang, H.; Bergeles, C.; Nelson, B. J. Characterizing the Swimming Properties of Artificial Bacterial Flagella. *Nano Lett.* **2009**, *9*, 3663–3667.
11. Ghosh, A.; Fischer, P. Controlled Propulsion of Artificial Magnetic Nanostructured Propellers. *Nano Lett.* **2009**, *9*, 2243–2245.
12. Tottori, S.; Zhang, L.; Qiu, F.; Krawczyk, K. K.; Franco-Obregon, A.; Nelson, B. J. Magnetic Helical Micromachines: Fabrication, Controlled Swimming, and Cargo Transport. *Adv. Mater.* **2012**, *24*, 811–816.
13. Gao, W.; Sattayasamitsathit, S.; Manesh, K. M.; Weihs, D.; Wang, J. Magnetically Powered Flexible Metal Nanowire Motors. *J. Am. Chem. Soc.* **2010**, *132*, 14403–14405.
14. Dreyfus, R.; Baudry, J.; Roper, M. L.; Fermigier, M.; Stone, H. A.; Bibette, J. Microscopic Artificial Swimmers. *Nature* **2005**, *437*, 862–865.
15. Zhang, L.; Petit, T.; Lu, Y.; Kratochvil, B. E.; Peyer, K. E.; Pei, R.; Lou, J.; Nelson, B. J. Controlled Propulsion and Cargo Transport of Rotating Nickel Nanowires near a Patterned Solid Surface. *ACS Nano* **2010**, *4*, 6228–6234.
16. Ogrin, F. Y.; Petrov, P. G.; Winlove, C. P. Ferromagnetic Microswimmers. *Phys. Rev. Lett.* **2008**, *100*, 218102.
17. Calvo-Marzal, P.; Sattayasamitsathit, S.; Balasubramanian, S.; Windmiller, J. R.; Dao, C.; Wang, J. Propulsion of Nanowire Diodes. *Chem. Commun.* **2010**, *46*, 1623–1624.

18. Chang, S. T.; Paunov, V. N.; Petsev, D. N.; Velev, O. D. Remotely Powered Self-Propelling Particles and Micropumps Based on Miniature Diodes. *Nat. Mater.* **2007**, *6*, 235–240.
19. Hong, Y.; Diaz, M.; Córdova-Figueroa, U. M.; Sen, A. Light-Driven Titanium-Dioxide-Based Reversible Microfireworks and Micromotor/Micropump Systems. *Adv. Funct. Mater.* **2010**, *20*, 1568–1576.
20. Liu, M.; Zentgraf, T.; Liu, Y.; Bartal, G.; Zhang, X. Light-Driven Nanoscale Plasmonic Motors. *Nat. Nanotechnol.* **2010**, *5*, 570–573.
21. Ibele, M.; Mallouk, T. E.; Sen, A. Schooling Behavior of Light-Powered Autonomous Micromotors in Water. *Angew. Chem., Int. Ed.* **2009**, *48*, 3308–3312.
22. Abid, J. P.; Frigoli, M.; Pansu, R.; Szeftel, J.; Zyss, J.; Larpent, C.; Brasselet, S. Light-Driven Directed Motion of Azobenzene-Coated Polymer Nanoparticles in an Aqueous Medium. *Langmuir* **2011**, *27*, 7967–71.
23. Stock, C.; Heureux, N.; Browne, W. R.; Feringa, B. L. Autonomous Movement of Silica and Glass Micro-objects Based on a Catalytic Molecular Propulsion System. *Chem.—Eur. J.* **2008**, *14*, 3146–3153.
24. Gibbs, J. G.; Zhao, Y. P. Autonomously Motile Catalytic Nanomotors by Bubble Propulsion. *Appl. Phys. Lett.* **2009**, *94*, 163104–3.
25. Solovev, A. A.; Mei, Y.; Bermúdez Ureña, E.; Huang, G.; Schmidt, O. G. Catalytic Microtubular Jet Engines Self-Propelled by Accumulated Gas Bubbles. *Small* **2009**, *5*, 1688–1692.
26. Gao, W.; Sattayasamitsathit, S.; Orozco, J.; Wang, J. Highly Efficient Catalytic Microengines: Template Electrosynthesis of Polyaniline/Platinum Microtubes. *J. Am. Chem. Soc.* **2011**, *133*, 11862–11864.
27. Pavlick, R. A.; Sengupta, S.; McFadden, T.; Zhang, H.; Sen, A. A Polymerization-Powered Motor. *Angew. Chem., Int. Ed.* **2011**, *50*, 9374–9377.
28. Golestanian, R.; Liverpool, T. B.; Ajdari, A. Propulsion of a Molecular Machine by Asymmetric Distribution of Reaction Products. *Phys. Rev. Lett.* **2005**, *94*, 220801.
29. Howse, J. R.; Jones, R. A. L.; Ryan, A. J.; Gough, T.; Vafabakhsh, R.; Golestanian, R. Self-Motile Colloidal Particles: From Directed Propulsion to Random Walk. *Phys. Rev. Lett.* **2007**, *99*, 048102.
30. Campuzano, S.; Orozco, J.; Kagan, D.; Guix, M.; Gao, W.; Sattayasamitsathit, S.; Claussen, J. C.; Merkoçi, A.; Wang, J. Bacterial Isolation by Lectin-Modified Microengines. *Nano Lett.* **2011**, *12*, 396–401.
31. Sundararajan, S.; Lammert, P. E.; Zudans, A. W.; Crespi, V. H.; Sen, A. Catalytic Motors for Transport of Colloidal Cargo. *Nano Lett.* **2008**, *8*, 1271–1276.
32. Balasubramanian, S.; Kagan, D.; Jack Hu, C.-M.; Campuzano, S.; Lobo-Castañon, M. J.; Lim, N.; Kang, D. Y.; Zimmerman, M.; Zhang, L.; Wang, J. Micromachine-Enabled Capture and Isolation of Cancer Cells in Complex Media. *Angew. Chem., Int. Ed.* **2011**, *50*, 4161–4164.
33. Burdick, J.; Laocharoensuk, R.; Wheat, P. M.; Posner, J. D.; Wang, J. Synthetic Nanomotors in Microchannel Networks: Directional Microchip Motion and Controlled Manipulation of Cargo. *J. Am. Chem. Soc.* **2008**, *130*, 8164–8165.
34. Hong, Y.; Blackman, N. M. K.; Kopp, N. D.; Sen, A.; Velegol, D. Chemotaxis of Nonbiological Colloidal Rods. *Phys. Rev. Lett.* **2007**, *99*, 178103.
35. Kagan, D.; Balasubramanian, S.; Wang, J. Chemically Triggered Swarming of Gold Microparticles. *Angew. Chem., Int. Ed.* **2011**, *50*, 503–506.
36. Campuzano, S.; Kagan, D.; Orozco, J.; Wang, J. Motion-Driven Sensing and Biosensing Using Electrochemically Propelled Nanomotors. *Analyst* **2011**, *136*, 4621–4630.
37. Jun, I.-K.; Hess, H. A Biomimetic, Self-Pumping Membrane. *Adv. Mater.* **2010**, *22*, 4823–4825.
38. Zhang, H.; Yeung, K.; Robbins, J. S.; Pavlick, R. A.; Wu, M.; Liu, R.; Sen, A.; Phillips, S. T. Self-Powered Microscale Pumps Based on Analyte-Initiated Depolymerization Reactions. *Angew. Chem., Int. Ed.* **2012**, *51*, 2400–2404.
39. Ozin, G. A.; Manners, I.; Fournier-Bidoz, S.; Arsenault, A. Dream Nanomachines. *Adv. Mater.* **2005**, *17*, 3011–3018.
40. Ebbens, S. J.; Howse, J. R. In Pursuit of Propulsion at the Nanoscale. *Soft Matter* **2010**, *6*, 726.
41. Erikson, K. R.; Fry, F. J.; Jones, J. P. Ultrasound in Medicine—A Review. *IEEE Trans. Sonics Ultrasonics* **1974**, *21*, 144–170.
42. Ziskin, M. C.; Petitti, D. B. Epidemiology of Human Exposure to Ultrasound: A Critical Review. *Ultrasound Med. Biol.* **1988**, *14*, 91–96.
43. Litvak, E.; Foster, K. R.; Repacholi, M. H. Health and Safety Implications of Exposure to Electromagnetic Fields in the Frequency Range 300 Hz to 10 MHz. *Bioelectromagnetics* **2002**, *23*, 68–82.
44. Kundt, A.; Lehman, O. Longitudinal Vibrations and Acoustic Figures in Cylindrical Columns of Liquids. *Annal Phys.* **1874**, 1.
45. King, L. V. On the Acoustic Radiation Pressure on Spheres. *Proc R. Soc., London* **1934**, *a147*, 212–40.
46. Rayleigh, J. W. On the Pressure of Vibrations. *Philos. Mag.* **1902**, *3*, 338–46.
47. Yosioka, K.; Kawasima, Y. Acoustic Radiation Pressure on a Compressible Sphere. *Acustica* **1955**, *5*, 167–73.
48. Shi, J.; Ahmed, D.; Mao, X.; Lin, S.-C. S.; Lawit, A.; Huang, T. J. Acoustic Tweezers: Patterning Cells and Microparticles Using Standing Surface Acoustic Waves (SSAW). *Lab Chip* **2009**, *9*, 2890–2895.
49. Wood, C. D.; Evans, S. D.; Cunningham, J. E.; O'Rorke, R.; Walti, C.; Davies, A. G. Alignment of Particles in Microfluidic Systems Using Standing Surface Acoustic Waves. *Appl. Phys. Lett.* **2008**, *92*, 044104.
50. Haake, A.; Dual, J. Contactless Micromanipulation of Small Particles by an Ultrasound Field Excited by a Vibrating Body. *J. Acoust. Soc. Am.* **2005**, *117*, 2752–2760.
51. Lee, W.; Amini, H.; Stone, H. A.; Di Carlo, D. Dynamic Self-Assembly and Control of Microfluidic Particle Crystals. *Proc. Natl. Acad. Sci. U.S.A.* **2010**, *107*, 22413–22418.
52. Oberti, S.; Neild, A.; Dual, J. Manipulation of Micrometer Sized Particles within a Micromachined Fluidic Device to Form Two-Dimensional Patterns Using Ultrasound. *J. Acoust. Soc. Am.* **2007**, *121*, 778–785.
53. Friend, J.; Yeo, L. Y. Microscale Acoustofluidics: Microfluidics Driven *via* Acoustics and Ultrasonics. *Rev. Mod. Phys.* **2011**, *83*, 647–704.
54. Wang, Z.; Zhe, J. Recent Advances in Particle and Droplet Manipulation for Lab-on-a-Chip Devices Based on Surface Acoustic Waves. *Lab Chip* **2011**, *11*, 1280–1285.
55. Oberti, S.; Möller, D.; Neild, A.; Dual, J.; Beyeler, F.; Nelson, B. J.; Gutmann, S. Strategies for Single Particle Manipulation Using Acoustic and Flow Fields. *Ultrasonics* **2010**, *50*, 247–257.
56. Shi, J.; Yazdi, S.; Steven Lin, S.-C.; Ding, X.; Chiang, I. K.; Sharp, K.; Huang, T. J. Three-Dimensional Continuous Particle Focusing in a Microfluidic Channel *via* Standing Surface Acoustic Waves (SSAW). *Lab Chip* **2011**, *11*, 2319–2324.
57. Martyn Hill, N. R. H., Ultrasonic Particle Manipulation. In *Microfluidic Technologies for Miniaturized Analysis Systems*; Steffen Hardt, F. S., Ed.; Springer: New York, 2007; pp 357−392.
58. Lim, W. P.; Yao, K.; Chen, Y. Alignment of Carbon Nanotubes by Acoustic Manipulation in a Fluidic Medium. *J. Phys. Chem. C* **2007**, *111*, 16802–16807.
59. Kong, X. H.; Deneke, C.; Schmidt, H.; Thurmer, D. J.; Ji, H. X.; Bauer, M.; Schmidt, O. G. Surface Acoustic Wave Mediated Dielectrophoretic Alignment of Rolled-up Microtubes in Microfluidic Systems. *Appl. Phys. Lett.* **2010**, *96*, 134105.
60. Smorodin, T.; Beierlein, U.; Ebbecke, J.; Wixforth, A. Surface-Acoustic-Wave-Enhanced Alignment of Thiolated Carbon Nanotubes on Gold Electrodes. *Small* **2005**, *1*, 1188–1190.
61. Shilton, R. J.; Glass, N. R.; Chan, P.; Yeo, L. Y.; Friend, J. R. Rotational Microfluidic Motor for on-Chip Microcentrifugation. *Appl. Phys. Lett.* **2011**, 98.
62. Hu, J.; Tay, C.; Cai, Y.; Du, J. Controlled Rotation of Sound-Trapped Small Particles by an Acoustic Needle. *Appl. Phys. Lett.* **2005**, *87*, 094104.
63. Bazou, D.; Castro, A.; Hoyos, M., Controlled Cell Aggregation in a Pulsed Acoustic Field. *Ultrasonics* in press.

64. Lierke, E. G. Acoustic Levitation—A Comprehensive Survey of Principles and Applications. *Acustica* **1996**, *82*, 220–237.
65. Woodside, S. M.; Bowen, B. D.; Piret, J. M. Measurement of Ultrasonic Forces for Particle−Liquid Separations. *AIChE J.* **1997**, *43*, 1727–1736.
66. Townsend, R. J.; Hill, M.; Harris, N. R.; White, N. M. Investigation of Two-Dimensional Acoustic Resonant Modes in a Particle Separator. *Ultrasonics* **2006**, *44*), e467–71.
67. Lilliehorn, T.; Simu, U.; Nilsson, M.; Almqvist, M.; Stepinski, T.; Laurell, T.; Nilsson, J.; Johansson, S. Trapping of Microparticles in the near Field of an Ultrasonic Transducer. *Ultrasonics* **2005**, *43*, 293–303.
68. Jensen, H. C. Production of Chladni Figures on Vibrating Plates Using Continuous Excitation. *Am. J. Phys* **1955**, *23*, 503–505.
69. Hobæk, H.; Nesse, T. L., Scattering from Spheres and Cylinders—Revisited. In *29th Scandinavian Symposium of Physical Acoustics*; Norwegian Physical Society: Oslo, Norway, 2006.
70. Bao, X.-L.; Cao, H.; Uberall, H. Resonances and Surface Waves in the Scattering of an Obliquely Incident Acoustic Field by an Infinite Elastic Cylinder. *J. Acoust. Soc. Am.* **1990**, *87*, 106–110.
71. Spengler, J. F.; Coakley, W. T.; Christensen, K. T. Microstreaming Effects on Particle Concentration in an Ultrasonic Standing Wave. *AIChE J.* **2003**, *49*, 2773–2782.
72. Wang, Y.; Hernandez, R. M.; Bartlett, D. J.; Bingham, J. M.; Kline, T. R.; Sen, A.; Mallouk, T. E. Bipolar Electrochemical Mechanism for the Propulsion of Catalytic Nanomotors in Hydrogen Peroxide Solutions. *Langmuir* **2006**, *22*, 10451–10456.
73. Moran, J. L.; Posner, J. D. Electrokinetic Locomotion Due to Reaction-Induced Charge Auto-Electrophoresis. *J. Fluid Mech.* **2011**, *680*, 31–66.
74. Anbar, M.; Pecht, I. On the Sonochemical Formation of Hydrogen Peroxide in Water. *J. Phys. Chem.* **1964**, *68*, 352–355.
75. Banholzer, M. J.; Li, S.; Ketter, J. B.; Rozkiewicz, D. I.; Schatz, G. C.; Mirkin, C. A. Electrochemical Approach to and the Physical Consequences of Preparing Nanostructures from Gold Nanorods with Smooth Ends. *J. Phys. Chem. C* **2008**, *112*, 15729–15734.
76. DaSilva, M.; Schneider, M. M.; Wood, D. S.; Kim, B.-J.; Stach, E. A.; Sands, T. D. The Use of Polyethyleneimine To Control the Growth-Front Morphology of Electrochemically Deposited Gold Nanowires for Engineered Nanogap Electrodes. *Small* **2009**, *5*, 2387–2391.
77. Ye, Z. A Novel Approach to Sound Scattering by Cylinders of Finite Length. *J. Acoust. Soc. Am.* **1997**, *102*, 877–884.
78. Honarvar, F.; Enjilela, E.; Sinclair, A. N. Correlation between Helical Surface Waves and Guided Modes of an Infinite Immersed Elastic Cylinder. *Ultrasonics* **2011**, *51*, 238–244.
79. Mitri, F. G. Acoustic Backscattering Enhancements Resulting from the Interaction of an Obliquely Incident Plane Wave with an Infinite Cylinder. *Ultrasonics* **2010**, *50*, 675–682.
80. Lenshof, A.; Magnusson, C.; Laurell, T. Acoustofluidics 8: Applications of Acoustophoresis in Continuous Flow Microsystems. *Lab Chip* **2012**, *12*, 1210–1223.
81. Khandpur, R. S. *Handbook of Biomedical Instrumentation*; McGraw-Hill Professional: New Delhi, India, 2003.
82. Barnett, S. B.; Ter Haar, G. R.; Ziskin, M. C.; Rott, H.-D.; Duck, F. A.; Maeda, K. International Recommendations and Guidelines for the Safe Use of Diagnostic Ultrasound in Medicine. *Ultrasound Med. Biol.* **2000**, *26*, 355–366.
83. Hernández, R. M.; Richter, L.; Semancik, S.; Stranick, S.; Mallouk, T. E. Template Fabrication of Protein-Functionalized Gold−Polypyrrole−Gold Segmented Nanowires. *Chem. Mater.* **2004**, *16*, 3431–3438.
84. Kline, T. R.; Tian, M.; Wang, J.; Sen, A.; Chan, M. W. H.; Mallouk, T. E. Template-Grown Metal Nanowires. *Inorg. Chem.* **2006**, *45*, 7555–7565.
85. Mbindyo, J. K. N.; Mallouk, T. E.; Mattzela, J. B.; Kratochvilova, I.; Razavi, B.; Jackson, T. N.; Mayer, T. S. Template Synthesis of Metal Nanowires Containing Monolayer Molecular Junctions. *J. Am. Chem. Soc.* **2002**, *124*, 4020–4026.